processes

MDPI

Article

Aerated Concrete, Based on the Ash of Thermal Power Plants, Nanostructured with Water-Soluble Fullerenols

Olga V. Rudenko [1], Nikolay A. Charykov [2,3], Natalya A. Kulenova [1,*], Marzhan A. Sadenova [1], Darya K. Anop [1] and Erzhan Kuldeyev [4]

[1] Priority Department Centre "Veritas" D. Serikbayev East Kazakhstan Technical University, 19 Serikbayev Str., Ust-Kamenogorsk 070000, Kazakhstan; orudenko@edu.ektu.kz (O.V.R.); msadenova@edu.ektu.kz (M.A.S.); dgalkina@edu.ektu.kz (D.K.A.)
[2] Department of Physical Chemistry, Saint Petersburg State Technological Institute (Technical University), 26 Moskovsky Ave., 190013 Saint Petersburg, Russia; ncharykov@yandex.ru
[3] Department of Physical Chemistry, Saint Petersburg State Electrotechnical University "LETI", ul. Professor Popov 5, 19376 Saint Petersburg, Russia
[4] Satbayev University, Satbayev St. 22a, Almaty 050013, Kazakhstan; e.kuldeyev@satbayev.university
* Correspondence: nkulenova@edu.ektu.kz

Abstract: This study is devoted to the synthesis of aerated concrete by a non-autoclave method using ash from thermal power plants and a nanopreparation. Fullerenol-m was used as a nanopreparation. The fullerenol-m content in the sealing water of aerated concrete changed in the range of 0.00 ÷ 0.03 mas.%. The main performance characteristics of the nanostructured aerated concrete were studied, namely the compressive strength, impact toughness, thermal conductivity, density and moisture content. A significant improvement in the performance characteristics of the nanomodified aerated concrete compared to unmodified samples was demonstrated, which was most clearly manifested as an increase in impact toughness by several (three to five) times. The best performance characteristics of the modified aerated concrete were observed at a fullerenol-m concentration relative to the added cement within 0.022–0.028 wt.%. The authors attribute such a strong change and improvement in the physical, chemical and operational properties of aerated concrete when modified with fullerenol-m to the fact that fullerenol-m (a few thousandths of wt.%) has a very strong structuring effect on the sealing water and, as a consequence, on the resulting aerated concrete.

Keywords: aerated concrete; non-autoclave method; ash and slag waste; cement; quicklime; fullerenol-m; compressive strength; impact strength; density; thermal conductivity

Citation: Rudenko, O.V.; Charykov, N.A.; Kulenova, N.A.; Sadenova, M.A.; Anop, D.K.; Kuldeyev, E. Aerated Concrete, Based on the Ash of Thermal Power Plants, Nanostructured with Water-Soluble Fullerenols. *Processes* **2024**, *12*, 2139. https://doi.org/10.3390/pr12102139

Academic Editor: Chin-Hyung Lee

Received: 26 August 2024
Revised: 19 September 2024
Accepted: 27 September 2024
Published: 1 October 2024

1. Introduction

The most popular building material in low-rise construction is aerated concrete, which is also called cellular concrete. The increase in the demand for aerated concrete is facilitated by the growth of electricity tariffs, and this in turn stimulates the use of building materials with low thermal conductivity [1]. Aerated concrete is used to construct partitions inside buildings, as well as for the insulation of external walls. It has good thermal insulation, which allows a reduction in the cost of heating a building. Over the past few decades, many authors have studied the possibility of improving the characteristics of various concretes using nanomaterials such as nano-TiO_2, nano-SiO_2 and carbon nanotubes [2–6]. Nanotechnology makes it possible to influence the properties of materials if the sizes of the nanomaterials are in the range of 1–100 nm (such a size can be fractional or fractal) [3], and this research topic is becoming increasingly popular among researchers due to the possibility of new scientific and practical applications [7,8]. The review in [9] presents new achievements in research related to increasing the durability of concrete using nanomaterials. It is shown that the inclusion of nanomaterials in concrete has a positive effect in terms of increasing its mechanical strength and durability, and it also leads to energy savings due

to reduced cement consumption in the production of concrete. It is known that in order to increase the strength and improve the pore structure in cellular concrete, it is possible to modify the composition with carbon-containing nanomaterials, the introduction of which results in the effect of reinforcing the viscous mineral matrix [10]. The work in [11] shows the effect of additives at ultra-low doses (0.006–0.042% by weight of the binder), such as dispersed multi-layer carbon nanotubes, in changing the physical and mechanical properties of cement concrete. Recently, much attention has been paid to the use of waste generated during coal combustion in thermal power plants as a silica component for the production of aerated concrete blocks. Attention has also been paid to the use of thermal power plant (TPP) ash as a filler for aerated concrete [12,13]. It should be noted that earlier, in [14], the possibility of modifying standard concrete and gypsum using water-soluble carbon nanomaterials was considered. The authors demonstrated a significant improvement in the strength characteristics of building materials (primarily the impact toughness).

This article is the first to investigate the possibility of using water-soluble carbon-containing nanopreparations for the production of aerated concrete by a non-autoclave method, using ash and slag waste from thermal power plants as a filler. The main objective of this study is to improve the main strength characteristics (and a number of others, such as the density, thermal conductivity and humidity).

This study has great potential, since the operation of TPPs results in the formation of a huge amount of ash and slag waste (ASW), which occupies huge areas and negatively affects the environment. The production of aerated concrete blocks based on ash and slag waste is associated with obvious environmental and economic advantages—the utilization of ash and slag waste from thermal power plants and the reduction of the costs of their maintenance and storage.

2. Materials and Methods of Material Synthesis

2.1. Concrete M400

For the preparation of aerated concrete samples, we used cement of the M400 brand, produced by the Bukhtarma Cement Company LLP. This is one of the most affordable cement grades used in the northeast of Kazakhstan and is produced on its own resource base. The chemical and phase compositions of M400 cement, as presented by the manufacturer, are given in Table 1.

Table 1. Average chemical and phase compositions of M400 cement (Bukhtarma Cement Company, Kazakhstan).

Name of Product	Content of Oxides (Mass. %)							
	SiO_2	Al_2O_3	Fe_2O_3	CaO	MgO	SO_3	$Na_2O + K_2O$	Others
Cement M400	23.74	4.67	3.68	64.82	1.63	0.21	0.87	0.38
Name of Product	**Content of Phases (Mass. %)**							
	$3CaO{\cdot}SiO_2$	$2CaO{\cdot}SiO_2$	$3CaO{\cdot}Al_2O_3$		$4CaO{\cdot}Al_2O_3{\cdot}Fe_2O_3$		CaO	
Cement M400	58.4	22.8	5.8		11.7		0.6	

Additionally, a fairly fast and reliable method for the analysis of various materials was used—the scanning electron microscopy (SEM) method. We conducted an electron microscopic study of M400 cement on a JSM-6390LV scanning electron microscope with an INCA microanalysis system. Figure 1 shows an image of the microstructure of the M400 cement and the quantitative composition of the chemical elements detected.

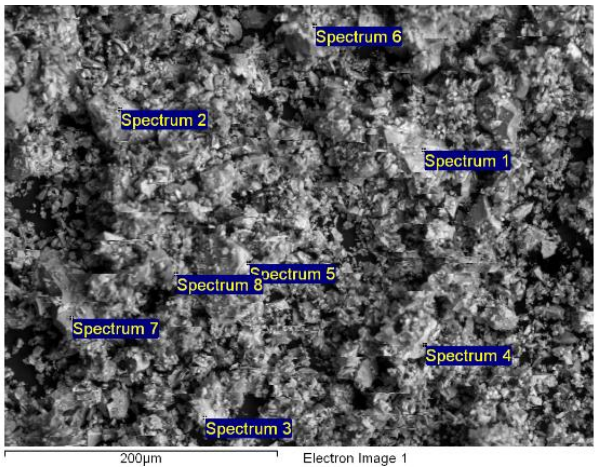

Name	Content of chemical elements (mass.%)										
Spectrum	O	Na	Mg	Al	Si	S	K	Ca	Fe	Cu	Zn
Spectrum 1	43.39	0.32	0.54	1.77	6.97	0.79	0.53	41.04	1.84	1.46	1.36
Spectrum 2	49.36	0.39	0.77	0.92	8.88	0.64	0.49	35.96	0.91	0.89	0.78
Spectrum 3	50.42	0.42	0.75	1.22	7.57	1.05	0.42	33.70	1.29	1.61	1.54
Spectrum 4	53.06	0.56	0.55	1.80	6.70	1.04	0.62	31.08	1.65	1.46	1.48
Spectrum 5	50.63	0.39	0.59	1.87	6.98	0.75	0.53	33.10	2.23	1.36	1.57
Spectrum 6	34.44		0.57	1.49	6.58	1.07	0.82	49.23	2.59	1.44	1.77
Spectrum 7	43.40	0.38	0.55	1.09	9.10	0.79	0.69	39.70	1.34	1.39	1.57
Spectrum 8	45.83	0.22	0.74	1.72	7.36	1.03	0.51	37.23	2.44	1.54	1.38

Figure 1. M400 cement analysis with JSM-6390LV scanning electron microscope and INCA microanalysis system (magnification: 300).

The main chemical elements are calcium, oxygen and silicon, which is confirmed by the data given in Table 1. Visually, the presence of these chemical elements in the studied sample of M400 cement is clearly visible in the energy spectrum obtained with the EDS microanalyzer (Figure 2).

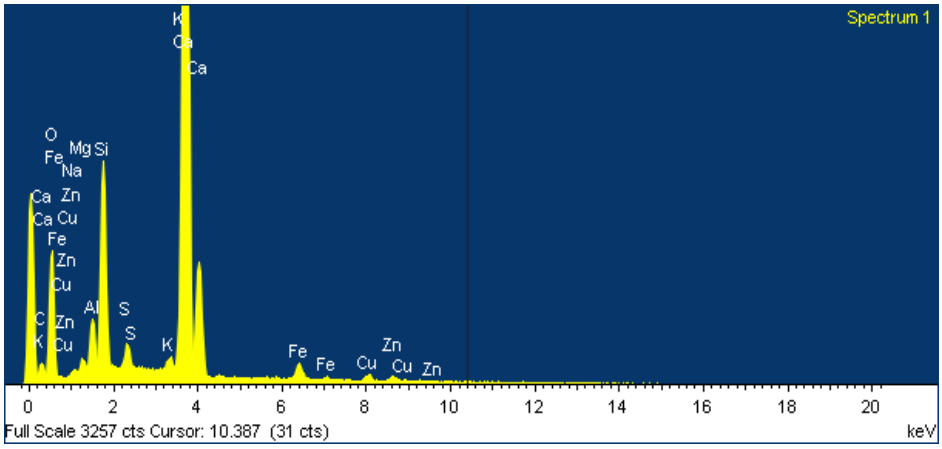

Figure 2. Results of element analysis via electron microscopy of M400 cement.

The presence of such elements as copper and zinc in the spectrum can be explained by the fact that the company uses waste slag from metallurgical plants in the Republic of Kazakhstan in the production of M400 cement.

2.2. Ash and Slag Waste—ASW

The authors used ash and slag waste (ASW; ash dump of boiler house No. 2 of Ust-Kamenogorsk Thermal Power Plant (Ust-Kamenogorsk, Kazakhstan)). This waste is not

only free but also has a negative cost, since it requires disposal. The results of the elemental analysis of the ASW are presented below in Table 2.

Table 2. Average chemical and phase analysis of ash and slag waste—ASW (ash dump of boiler room No. 2 of Ust-Kamenogorsk Thermal Power Plant (Ust-Kamenogorsk, Kazakhstan)).

Name of Product	Content of Oxides (Mass.%)								
	SiO_2	Al_2O_3	Fe_2O_3	CaO	MgO	TiO_2	$Na_2O + K_2O$	SO_3	Others
ASW	47.08	33.52	4.99	2.94	1.27	0.92	2.15	0.78	5.35

Ash and slag waste is characterized by a complex composition. In terms of the chemical composition, the basis of ash and slag waste is silicon, aluminum and iron oxides. The content of alkali and alkaline earth metal oxides is approximately 6.4%. We additionally conducted an electron microscopic study of the ash and slag waste using the JSM-6390LV scanning electron microscope with the INCA microanalysis system. Figure 3 shows an image of the ash and slag waste microstructure and the quantitative composition of the chemical elements detected.

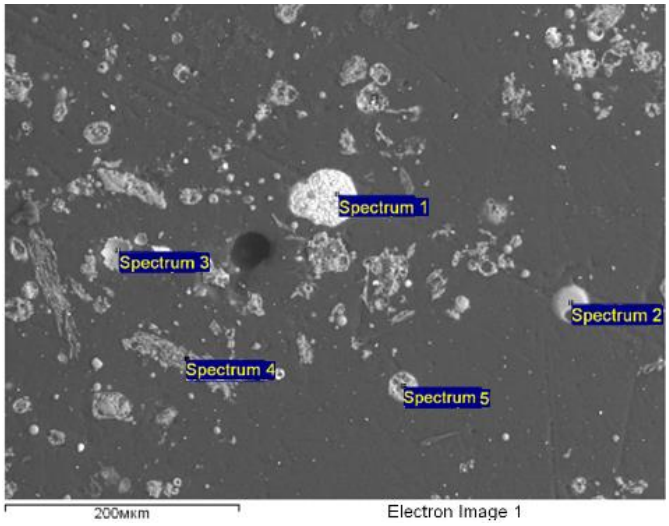

Number	Content of chemical elements (mass.%)							
	O	Na	Al	Si	K	Ca	Ti	Fe
Spectrum 1	48.14		7.96	16.98		6.15		19.55
Spectrum 2	55.08		15.47	20.84		4.00		4.62
Spectrum 3	56.48		13.47	22.41	1.55	2.01		4.38
Spectrum 4	58.82		12.74	28.44				2.63
Spectrum 5	57.43	1.36	13.74	18.92	0.92	2.43	2.58	19.35

Figure 3. Ash and slag waste (ASW) analysis using JSM-6390LV scanning electron microscope with INCA microanalysis system (magnification: 300).

In addition to aluminosilicate aggregates, the composition of fly ash includes spheroidal particles of magnetite (Fe_3O_4) mixed with hematite (Fe_2O_3), which constitute the magnetic fraction of ASW.

Figure 4 shows the X-ray diffraction pattern of the ASW obtained using an Aeris Research diffractometer.

The comparison of the study results with the diffraction database showed that the studied sample of ASW was represented by the following: amorphous phase—38.1%; mullite—21.0%; quartz—38.5%; magnesioferrite—1.5%; magnetite—0.1%; hematite—0.8%.

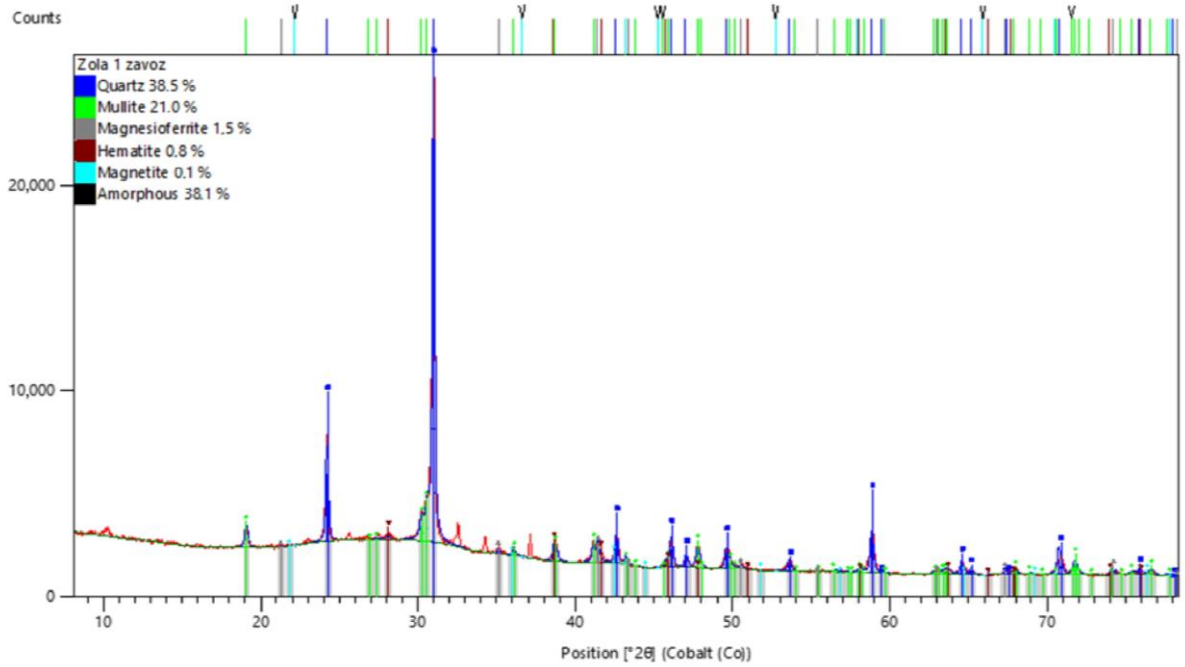

Figure 4. X-ray diffraction spectrum of ASW sample obtained on an Aeris Research diffractometer.

2.3. Fullerenol-m

By themselves, individual, well-purified fullerenols (for example, probably the most popular fullerenol, C_{60} $(OH)_{24}$; C_{70} $(OH)_{12}$) [15,16] are quite expensive and cannot be effectively used in construction, even in the form of microadditives. Therefore, in our work, we used the much more accessible fullerenol-m. This nanopreparation was obtained using a previously developed method for the synthesis of mixed fullerenols (fullerenol-mix-ss) directly from fullerene soot [17]. Hence, the name of the nanopreparation used is fullerenol-mix or fullerenol-m. The stages in the synthesis of fullerenol-m and the characteristics of the intermediates at the different stages of synthesis are presented in Table 3. The research on this product was carried out via a number of methods associated with physicochemical analysis (Table 4, Figures 5–11).

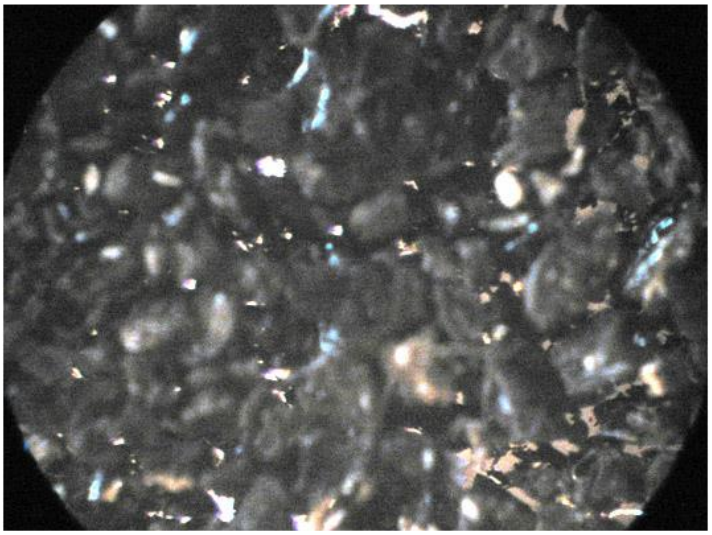

Figure 5. Optical microscopy photo (magnification: 50) of crystals of fullerenol-m.

Table 3. Stages and characteristics of *fullerenols-m* synthesis.

Stage Number	Synthesis Stage	Stage Characteristics
1.	Reaction for fullerenol-m preparation	
1.1.	Fullerene soot	Plasma-arc erosion of graphite rods in He atmosphere (method W. Kratschmer [18–22], type of construction [23]). Fullerene content: sum of fullerenes = 12.4 ± 0.3 mass.% from soot mass; C_{60} = 73 ± 2, C_{70} = 25 ± 2, C_{76} + C_{78} + C_{84} + . . . ≈ 1.5 ± 0.5 mass.% from sum fullerene mass. In experiment, always below m_{soot} = 1000 mg.
1.2.	NaOH water solution	Solution volume V = 100 cm^3, concentration C_{NaOH} = 10 mass.%, reactive purity ≥ 99.5 mass.%
1.3	Interphase catalyst $[(n-C_4H_9)_4]OH$ water solution	Solution volume V_{cat} = 0.5 cm^3, solution concentration C_{cat} = 8 mass.%, reactive purity ≥ 98 mass.%
2.	Reactive mixing, conducting reaction process	Shaker thermostat ($T = 25 \pm 0.2$ °C); magnetic stirrer ($\widetilde{\omega}$ = 4 Hz); time of reaction t = 7 days.
3.	Filtration of reactive solution	Blue ribbon (pores $d \approx 2 \div 3$ μm)
4.	Evaporation of solution	Rotary vacuum evaporator (≈ 20 mm Hg), ratio of solution volume ≈ 1/12
5.	Acidification of solution	Acidification agent HCl; concentration $C_{acid} \approx 36$ mass.%; $pH \approx 1.5$ *a.u.*; standing time = 3 h
6.	Precipitation of target product with methanol	CH_3OH volume ≈ 50 cm^3. Sediment extraction by filtration (blue ribbon)
7.	Water–methanol recrystallization	10 cm^3 (H_2O − HCl solution)/20 cm^3 (CH_3OH),filtration triple process, pH water solution $pH \approx 1.5$ *a.u.*
8.	Soft drying of target product	Vacuum dry box, T = 50 °C, P = 10 mmHg; t = 5 h

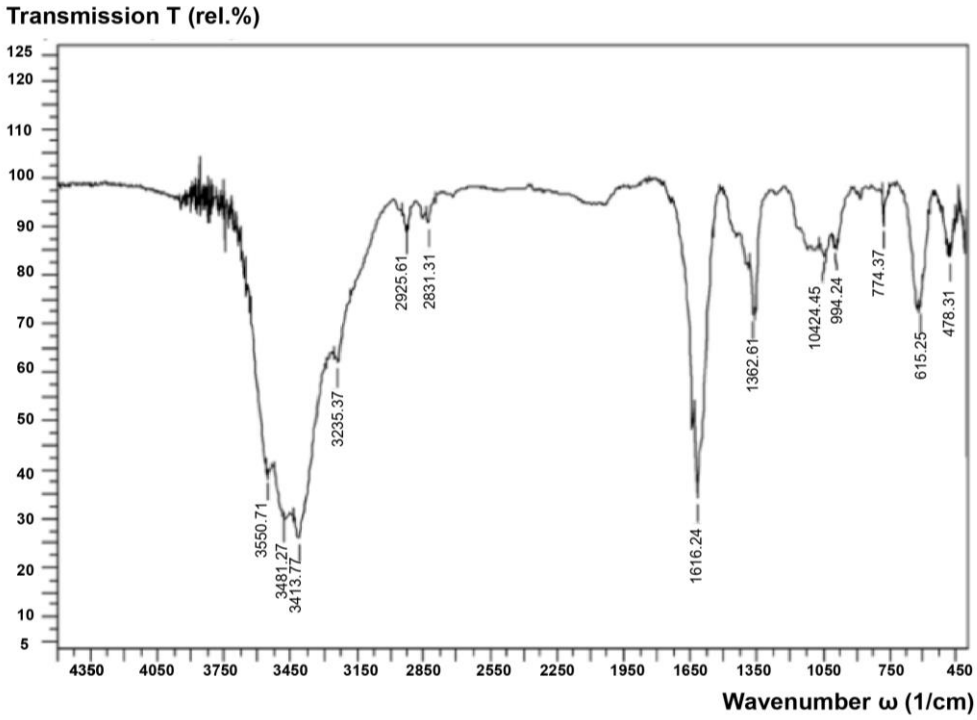

Figure 6. IR spectrum of fullerenol-m.

Table 4. Physical–chemical investigation of fullerenol-m product.

Method of Physical–Chemical Analysis	Results of Analysis
C/H/N Analyzer 5E-CHN2200	Content in mass % (C = 66, H = 2, O = 32 (difference)). Average molecular weight is $\overline{M} = 1140 \pm 40\ at.un.$
Electronic microscopy, VEGA-3 TESCAN (XRF Analyzer)	Content in mass % (C = 65, H = 2 (difference), O = 31, Na = 2).
Optical microscopy, Min-5	Magnification $(10 \div 1000)$ (Figure 5)
Mass spectrometry, Mibcrotof (Bruker), ionization–electronic impact	Reflexes of adducts $C_n(OH)_mO_p(ONa)_q$: $(n = 60[\approx 73\ \text{mol.\%}], n = 70[\approx 25\ \text{mol.\%}],$ $= 76, 78, 84 \ldots [\approx 2\ m(\text{mol.\%}], m = 16 \div 30, p = 2 \div 3, q = 0 \div 2)$. Reflexes at values (M/Z = 925–1163 a.e., single-charged anions) (Figure 8)
Infrared spectrophotometry, Shimadzu FTIR8400S $\left(\widetilde{\nu} = 400 \div 4000\ \text{cm}^{-1}, KBr\right)$	$\widetilde{\nu}_v$(O-H) $= 3410 \div 3450\ \text{cm}^{-1}$; $\widetilde{\nu}_v$(C-O) $= \div 1060 \pm 15\ \text{cm}^{-1}$; $\widetilde{\nu}_\delta$(C-O-H) $= \div 1370 \pm 10\ \text{cm}^{-1}$; $\left(\widetilde{\nu}_{v-fullerene\ core} =\right.$ 1597, 1440, 880, 714, 697 etc cm^{-1}; v—valence oscillations, δ—deformation oscillations (Figure 6)
Electronic spectrophotometry, SPECORD M-32; λ = 200–1110 nm; standard—water	Absence of adsorption peaks. Booger–Lambert–Beer light absorption law (optical way l = 1 cm; wavelength = 330 cm): $C_{fullerenol-m}\left(\frac{g}{dm^3}\right) = 5.11D_{330}$ (Figure 7)
Dynamic light scattering, Malvern Zetasizer Nano ZS90 apparatus	Diameters of different orders of spherical associates: 0-order, $\delta \approx 2\ \text{nm} - absence$; I − order − monomers, $\delta \approx 25 \pm 10\ \text{nm} - \left(C_{fullerenol-m} = 0.05 \div 0.15\ \text{g/dm}^3\right)$; II − order, $\delta \approx 230 \pm 50\ \text{nm} - \left(C_{fullerenol-m} = 0.15 \div 3.0\ \text{g/dm}^3\right)$; III − order − microcolloidsolution, $\delta \approx 3 \pm 1\ \text{nm} - \left(C_{fullerenol-m} = 3.0 \div 10\ \text{g/dm}^3\right)$ (Figure 11)
Solubility in water, method of isotherm saturation in ampoules; time of saturation = 8 h; magnetic stirrer	Solubility of fullerenol − m in g/dm^3at temperature 0 °C − 57; 25 °C − 111; 50 °C − 137; 80 °C − 153.
Complex thermal analysis, Shanghai Jiahang Instruments Co., Ltd.; air atmosphere, normal pressure, temperature range $T = 25 \div 115$ °C	Decomposition of crystal hydrate of fullerenol − m ($T = 100 \div 13$ °C); oxidative destruction of fullerenol − m, consists of processes of dehydroxylation and decarboxylation, with formation of semi − ketones and rearrangement of hydroxyl groups of pinacol type and their degradation ($T = 170 \div 83$ °C); loss of all hydroxyl groups ($T = 850 \div 880$ °C); oxidation of fullerene cores = ($T \geq 900$ °C) (Figure 9)
Nuclear magnetic resonance; C^{13}; NMR Bruker; standard—TMS	Reflexes in ppm : 142, 152, 148, 131 (C_{60} and C_{70} non-hydroxylated cores); 76 (hydroxylated carbon atom in C_{60} *core*); 83 (hydroxylated carbon atom in C_{70} *core*).
Refraction index of water solutions at 20 °C; HRK 9000 A	Refraction indexes : $n_{20}^D\left(C_{fullerenol-m} = 10\ \text{g/dm}^3\right) = 1.3361$; $n_{20}^D\left(C_{fullerenol-m} = 20\ \text{g/dm}^3\right) = 1.3379$; $n_{20}^D\left(C_{fullerenol-m} = 50\ \text{g/dm}^3\right) = 1.3388$.
High-performance liquid-phase chromatography; HPLC system, Agilent 1200; column, Agilent Zorbax SB-C18 (4.6 mm × 150 mm, dimension of particles, 5 μm); eluent, water–acetonitrile (1/20); detection, spectrophotometry at $\lambda = 330, 280$ nm	Detected at time t = 1.6 min weak peak of impurities (≈1.2 *square*%); t = 2.6 min strongest peak of $fullerenol - m$ (≈99 *square*%). Main peak width at the half − height $d_{1/2} \approx$ 0.25 min. Chromatographic purity of $fullerenol - m \approx 98 \div 99$ mass. % (Figure 10).

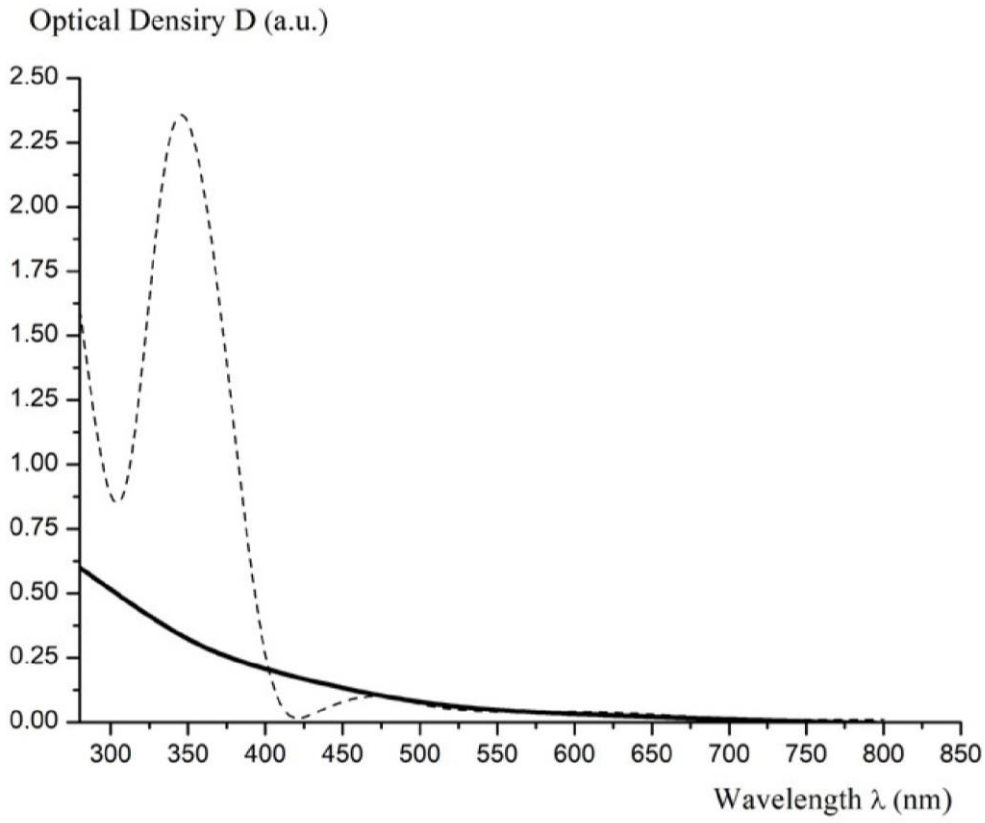

Figure 7. Electronic spectrum of fullerenol-m (solid line); spectrum of C_{60}—dot.

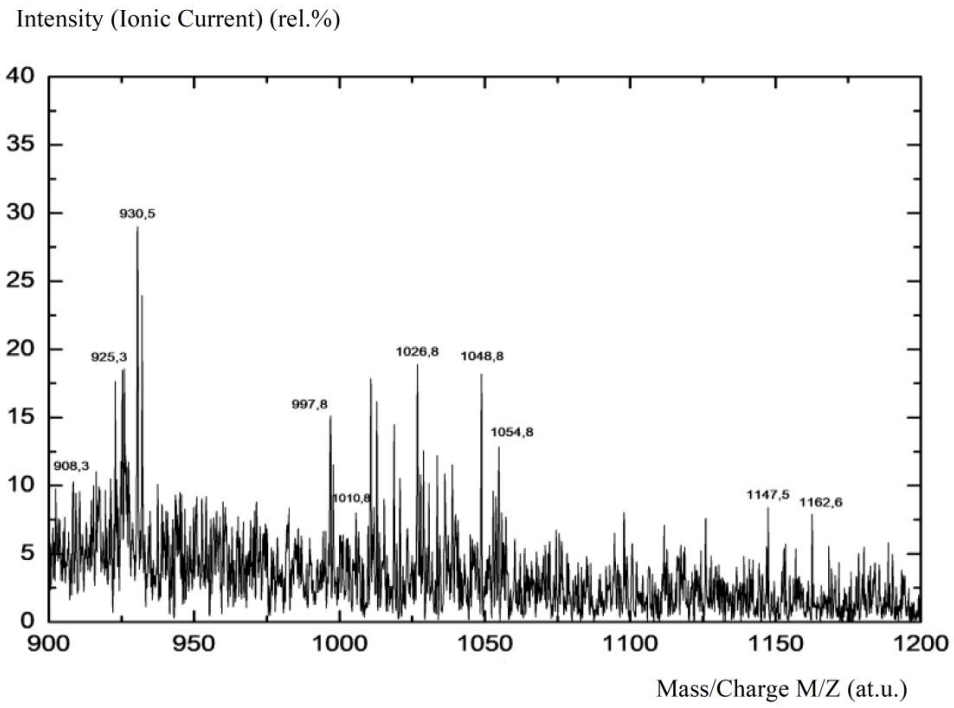

Figure 8. Mass spectrum of fullerenol-m (fragment).

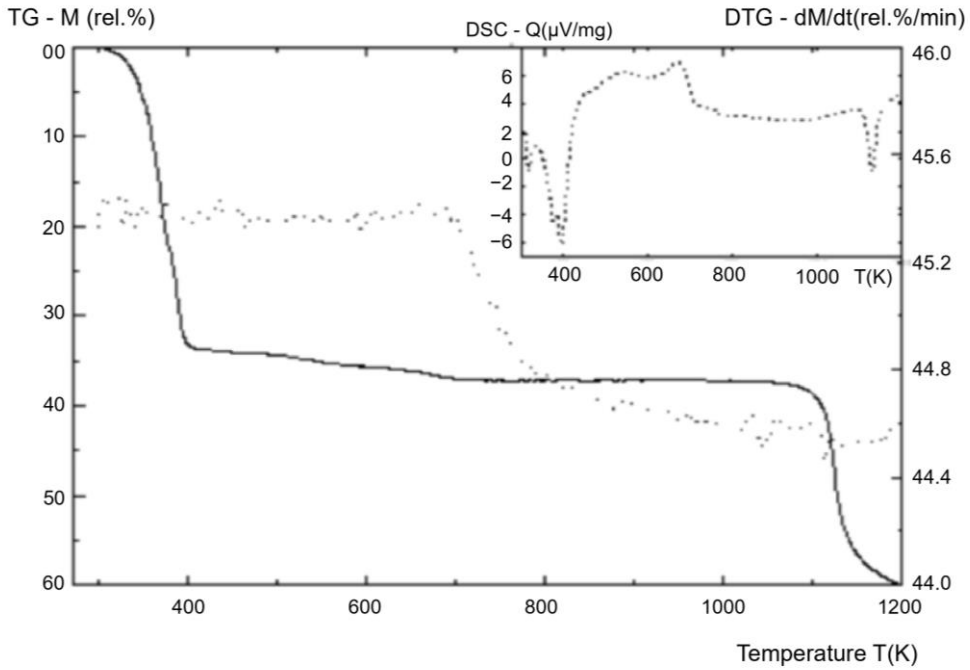

Figure 9. Thermogram of fullerenol-m (TG curve—solid, DTG curve—points).

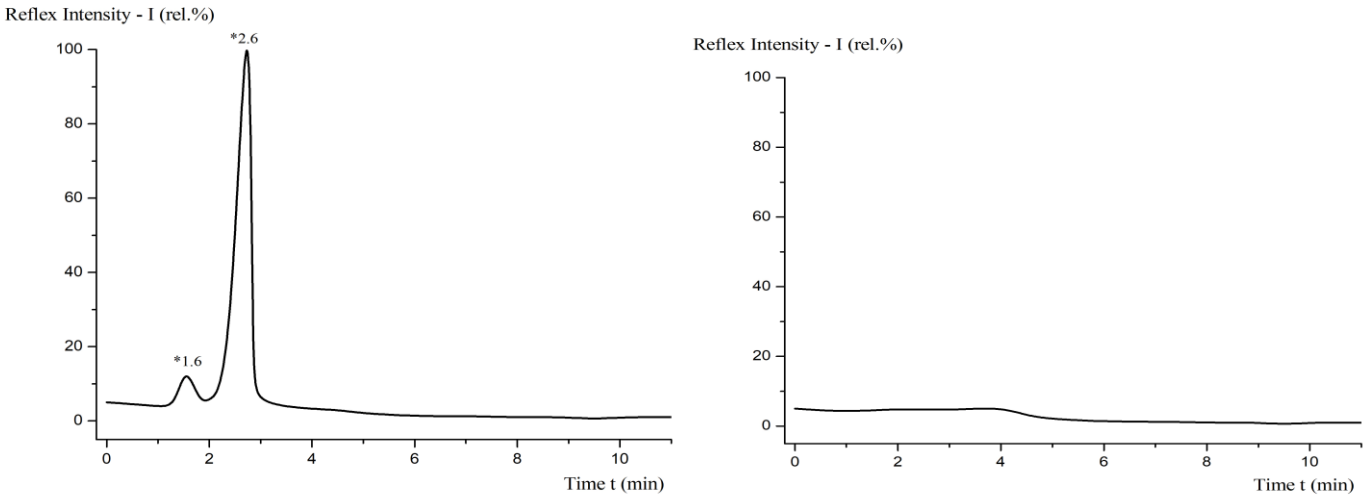

(**a**) (**b**)

Figure 10. HPLC of the solution of fullerenol-m (**a**); basic line without fullerenol-m (**b**).

According to Figure 5 (optical microscope Min-5), the morphology of fullerenol-m corresponds to a three-dimensionally soldered polycrystalline formation with an average linear crystallite size of several hundred microns. The linear size of the soldered crystallite in the photo of 1 cm corresponds to a real size of about 200 microns. The fullerenol-m synthesized by us was studied for identification by infrared spectrophotometry using a Shimadzu FTIR8400S device (Figure 6 and Table 4). The study of the obtained spectrum allowed us to identify the main absorption peaks at the given frequencies, corresponding to the O-H, C-O and C-O-H groups (Table 4).

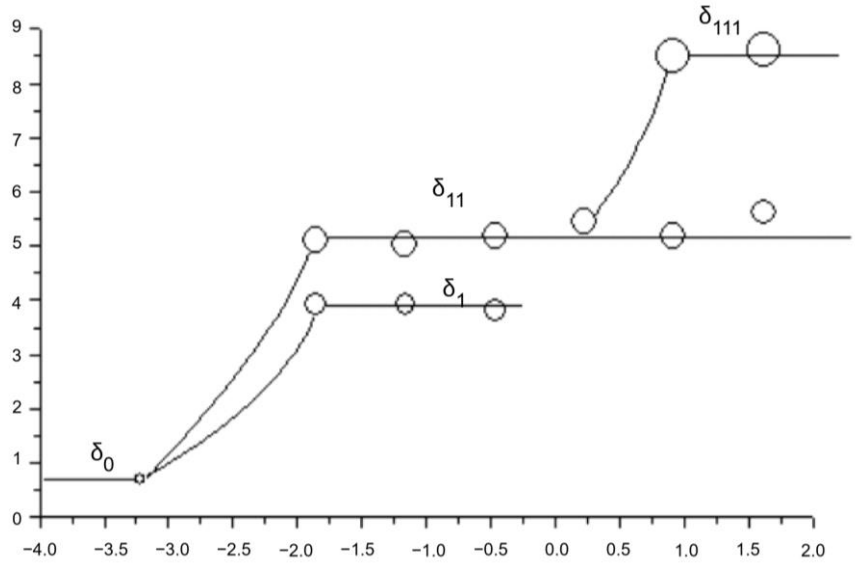

Figure 11. Dynamic light scattering of the solution of fullerenol-m (associate size distribution).

The data on the identification of fullerenol-m using the SPECORD M-32 electron spectrometer are presented in Table 4 and Figure 7.

As can be clearly seen from Figure 7, the electron spectrum of fullerenol-m has no visible absorption peaks, and only monotonously increasing absorption is observed when shifted to the short-wavelength region of the spectrum. In particular, there is no intense absorption peak common to light fullerenes at λ = 335.7 nm (see the electronic absorption spectrum for the solution of C_{60}, represented in Figure 7, for comparison).

Using mass spectrometry with the Mibcrotof device (Bruker), ionization–electronic impact studies were conducted to identify fullerenol-m, the results of which are presented in Table 4 and Figure 8.

Figure 8 clearly shows the presence of mass-spectrometric peaks at M/Z = 925–1163 a.u., corresponding to sodium forms of polyalcohols Cn(OH)mOp(ONa)q. The study of the thermal stability of fullerenol-m was carried out using a device for the thermal testing of materials from Shanghai Jiahang Instruments Co., Ltd., in an air atmosphere at normal pressure in the temperature range T = 25 ÷ 1150 °C (the results are presented in Table 4 and Figure 9).

The thermogram shows that, at T = 100 ÷ 130 °C, the decomposition of the fullerenol-m crystal hydrate occurs. At T = 170 ÷ 830 °C, the oxidative destruction of fullerenol-m occurs, consisting of dehydroxylation and decarboxylation processes, with the formation of semi-ketones and the rearrangement of the pinacol-type hydroxyl groups and their degradation. At T = 850 ÷ 880 °C, the loss of all hydroxyl groups is observed; at $T \geq$ 900 °C, the oxidation of the fullerene nuclei begins.

Figure 10 shows the HPLC of the solution of fullerenol-m (a); in the basic line without fullerenol-m (b), it was removed using an Agilent liquid chromatograph. Table 4 shows the experimental conditions.

In Figure 10, it can be found that, at t = 2.6 min, the strongest peak of fullerenol-m is observed. The width of the main peak at half-height is d_(1/2) ≈ 0.25 min. The chromatographic purity of fullerenol-m is ≈ 98 ÷ 99 wt%.

Figure 11 and Table 4 show the data on the size distribution of the associates, obtained using the Malvern Zetasizer Nano ZS90 device.

The classical stage-by-stage hierarchical association of nanoclusters formed by molecules creating a mixed nanopreparation of fullerenol-m was found. Here, zeroth-

order associates (monomers with linear dimensions $\delta \approx 2$ nm) at the lowest gross concentrations of fullerenol-m are found; at $C_{fullerenol\text{-}m} < 0.01$ g/dm^3, first-order associates with $\delta \approx 25 \pm 10$ nm are formed; at $C_{fullerenol\text{-}m} = 0.05 \div 0.15$ g/dm^3, second-order associates with $\delta \approx 230 \pm 50$ nm are formed from first-order associates; at $C_{fullerenol\text{-}m} = 0.15 \div 3.0$ g/dm^3, third-order associates with $\delta \approx 3 \pm 1$ nm are formed from second-order associates; and at $C_{fullerenol\text{-}m} = 3.0 \div 10$ g/dm^3, a microcolloid solution is formed, based on third-order associates.

2.4. Aerated Concrete

For the synthesis of aerated concrete, the following reagents were additionally used: technical grade A soda ash with sodium carbonate containing at least 99.4% Na_2CO_3; grade A5 aluminum powder; and fullerenol-m.

The research methodology included the production and testing of experimental aerated concrete samples (cubes with an edge size of 15 cm) with different amounts of fullerenol-m, including control samples (with a three-fold repetition of the experiment). The scheme of the synthesis process is presented in Figure 12.

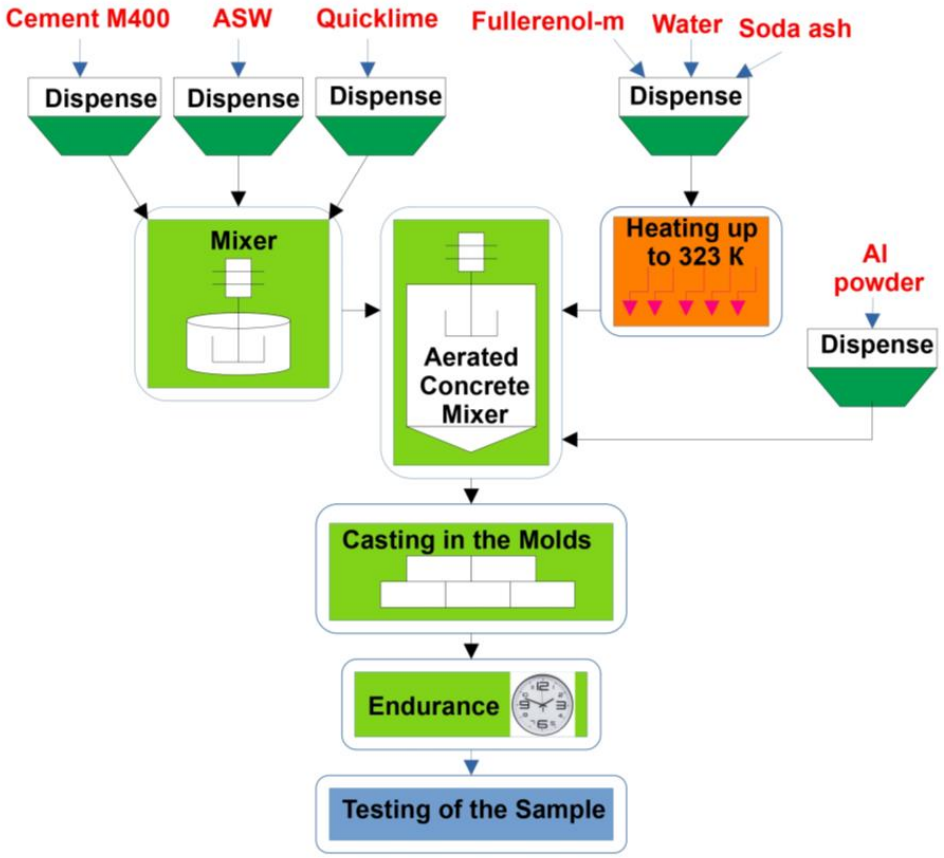

Figure 12. The scheme of the synthesis of aerated concrete, based on the ash of thermal power plants, nanostructured with water-soluble fullerenols.

Concrete, ASW and other dry materials were dosed by weight (Figure 12). First, cement, ASW and quicklime were mixed. Separately, a mixing solution was prepared containing fullerenol-m at the required concentration [16], soda ash (Na_2CO_3) and water. Then, the mixing solution was heated to 50 °C. The heated mixing solution was added to the dry mixture consisting of cement, ASW and quicklime and mixed for 3 min. After this, aluminum powder was added to the resulting mixture and mixed for 2 min. When the aluminum powder was introduced into the liquid suspension, active gas formation began, due to which pores were formed. The finished mixture was poured into molds

to two thirds of the height. The lifting of the aerated concrete and the minimum gain in strength occurred under normal conditions; then, the samples were placed in a normal curing chamber for storage for 28 days.

In our experiments, we used different ratios of ASW, cement and lime:

- cement/slag waste/lime 1.0/1.0/0.0 (in grams 2200/2200/0);
- cement/slag waste/lime 1.0/0.9/0.1 (in grams 2200/1980/220);
- cement/slag waste/lime 1.0/0.8/0.2 (in grams 2200/1760/440).

The amounts of soda ash and aluminum powder in all experiments were the same at 10 g and 3.6 g, respectively. The volume of the mixing solution in the experiments was 2450 mL.

Figure 13 shows the appearance of the aerated concrete samples obtained by the non-autoclave method with the same concentration of fullerenol-m (0.028 wt.% in relation to cement).

Figure 13. The appearance of aerated concrete obtained by a non-autoclave method with the same concentration of fullerenol-m (0.028 mass.% relative to cement).

Figure 14 shows an image of the microstructure of the synthesized aerated concrete sample, obtained using an electron microscope. Table 5 shows the minimum and maximum concentrations of the chemical elements found in the aerated concrete when examined using the scanning electron microscopy method.

Table 5. Average chemical analysis of aerated concrete, with maximum and minimum element content.

Element	Content (Mass.%)										
	O	**Na**	**Mg**	**Al**	**Si**	**P**	**S**	**K**	**Ca**	**Ti**	**Fe**
Max	64	1.5	1.8	13	18	0.6	0.5	1.2	28	0.6	2.3
Min	56	0.6	0.3	2.4	4.9	0.6	0.2	0.3	5.3	0.2	1.1

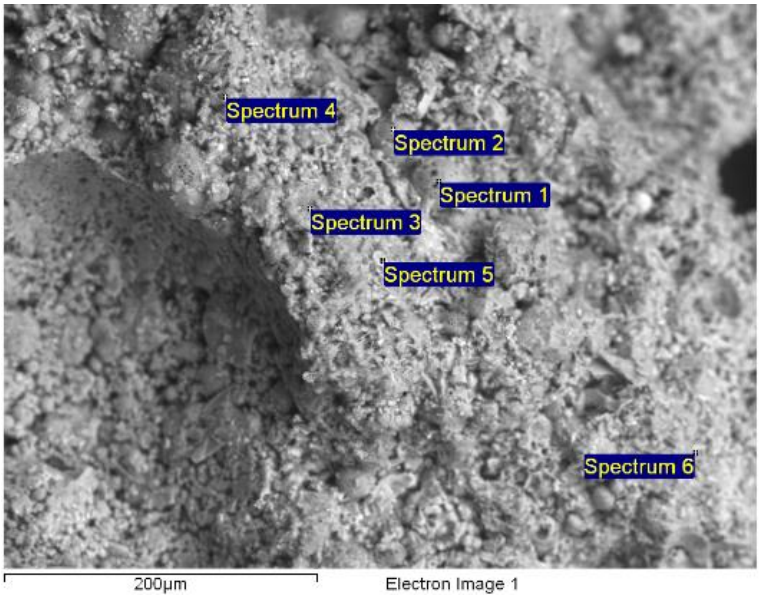

Figure 14. Aerated concrete analysis using JSM-6390LV scanning electron microscope with INCA microanalysis system (magnification: 300).

The main chemical elements are oxygen, calcium, aluminum and silicon. Visually, the presence of the chemical elements in the studied sample of aerated concrete was confirmed by the energy spectrum obtained with the EDS microanalyzer (Figure 15).

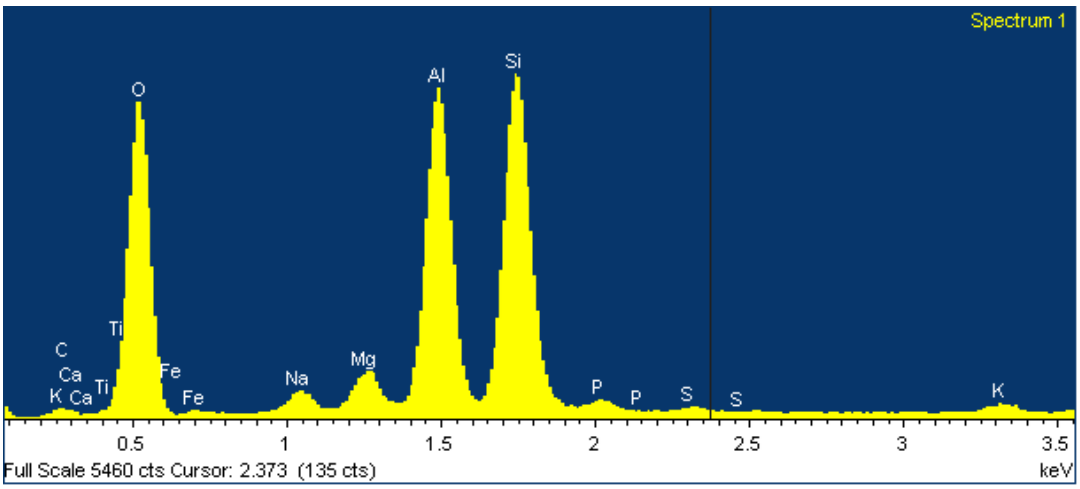

Figure 15. The results of the element analysis of the aerated concrete using an electron microscope (example).

2.5. Testing and Research Methods

2.5.1. Specific Impact Strength

The classical methods of Charpy and Izod are rarely applied to construction materials, i.e., cement/beton, because of the relatively low impact strength and high mechanical heterogeneity of the latter. In the testing of cement/beton by these methods, it is practically impossible to obtain stable and internally correlated results. For the impact resistance testing of nanomodified construction material samples, we used a method that was methodically close to Gardner's test (method of falling metal ball) [24]. The scheme of the apparatus is shown in Figure 16. As a result, we obtained data on the so-called specific impact resistance, which has the unit [kJ/m^3], or the classical impact resistance in ·m^{-1}.

We determine the so-called first specific impact resistance (when the first crack appears) and the second one (when complete sample destruction is observed).

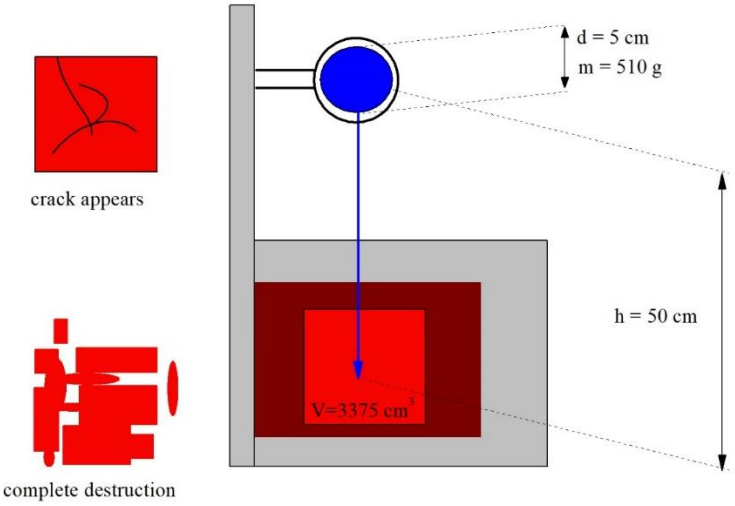

Figure 16. Schematic of the device for the measurement of the specific impact resistance. Falling spherical steel weight (blue), r—weight radius, m—weight mass, h—drop height; gray parallelepiped—platform; brown parallelepiped—stop inserter of the sample; red cube—aerated concrete sample with the volume V = 15·15·15 = 375 cm^3. Schematic images of samples: with crack (top left), with complete destruction (bottom left).

2.5.2. Compressive Strength

Compressive strength tests of the samples were carried out using a PGM-100MG4 hydraulic press (small-sized hydraulic press, Russian [25]). The measurements were carried out in accordance with [26]. Axis compression cubes with certain dimensions (≈150 mm × 50 mm × 150 mm) were studied.

2.5.3. Density

The density of the aerated concrete was determined by the direct weighing of the cubes, taking into account the imperfection of the shape (average of 3 measurements).

2.5.4. Humidity

The humidity of the aerated cement was measured by a humidity meter, the electronic moisture meter MG4-U [27]. The measurements were carried out in accordance with [28].

2.5.5. Thermal Conductivity

The thermal conductivity of the aerated cement was measured by a thermal conductivity meter ITP-MG4 [29]. The measurements were carried out in accordance with [29].

3. Results

The strength characteristics and some physical–chemical properties of the aerated concrete nanostructured with fullerenols are presented in Table 6 and Figures 17 and 18.

Table 6. Strength characteristics and some physical–chemical properties of aerated concrete nanostructured with fullerenols.

Mass Ratio: Cement/ ASW/Quicklime	Fullerenol Content in Sealing Water of Aerated Concrete (Mass.%)								Standard Deviation Limits (Min–Max)
	0.0000	0.0075	0.0100	0.0125	0.0150	0.0200	0.0250	0.0300	
Specific strength before crack appears—SS-a (cubes) (kJ/m^3)									
1.0/1.0/0.0	3.68	4.46	6.61	8.86	10.95	14.88	17.75	17.01	0.33–0.56
1.0/0.9/0.1	5.23	5.97	8.11	11.31	13.88	17.16	19.26	18.63	0.36–0.48
1.0/0.8/0.2	7.39	8.17	11.04	15.58	18.73	22.05	24.26	23.64	0.34–0.49
Specific strength for complete destruction—SS-c (cubes) (kJ/m^3)									
1.0/1.0/0.0	8.10	9.67	11.75	14.03	18.24	23.07	28.10	27.36	0.39–0.57
1.0/0.9/0.1	13.45	14.92	17.70	20.36	22.64	28.20	31.11	29.80	0.38–0.61
1.0/0.8/0.2	18.47	20.05	23.54	27.46	30.71	36.90	40.44	39.15	0.31–0.58
Coefficient of impact strength CI = SS-c/SS-a (a.u.)									
1.0/1.0/0.0	2.2	2.2	1.8	1.6	1.7	1.7	1.6	1.6	0.03–0.20
1.0/0.9/0.1	2.6	2.5	2.2	1.8	1.6	1.6	1.6	1.6	0.06–0.2
1.0/0.8/0.2	2.5	2.5	2.1	1.8	1.6	1.7	1.7	1.7	0.02–0.26
Compressive strength—CS (cube) (MPa)									
1.0/1.0/0.0	0.85	0.89	0.96	1.02	1.08	1.15	1.18	0.94	0,11–0,15
1.0/0.9/0.1	1.23	1.28	1.32	1.38	1.41	1.51	1.61	1.33	0.11–0.14
1.0/0.8/0.2	1.39	1.44	1.48	1.56	1.52	1.64	1.80	1.49	0,10–0,14
Density—D (kg/m^3)									
1.0/1.0/0.0	671	645	638	625	611	588	564	591	3.0–6.5
1.0/0.9/0.1	682	661	645	633	623	602	575	597	3.1–6.0
1.0/0.8/0.2	695	673	661	654	647	628	611	629	2.6–6.5
Humidity—H (mass. %)									
1.0/1.0/0.0	11.8	10.4	8.9	6.5	5.9	5.4	9.1	11.5	0.14–0.41
1.0/0.9/0.1	9.2	8.8	7.5	5.8	4.8	4.0	7.1	8.8	0.21–0.30
1.0/0.8/0.2	7.3	6.8	6.0	4.7	4.1	3.1	5.2	6.6	0.32–0.47
Thermal conductivity—λ, W/(m·K)									
1.0/1.0/0.0	0.157	0.151	0.149	0.147	0.143	0.135	0.124	0.127	0.01–0.02
1.0/0.9/0.1	0.160	0.155	0.151	0.148	0.144	0.137	0.128	0.131	0.01–0.02
1.0/0.8/0.2	0.163	0.158	0.155	0.154	0.151	0.148	0.145	0.147	0.01–0.02

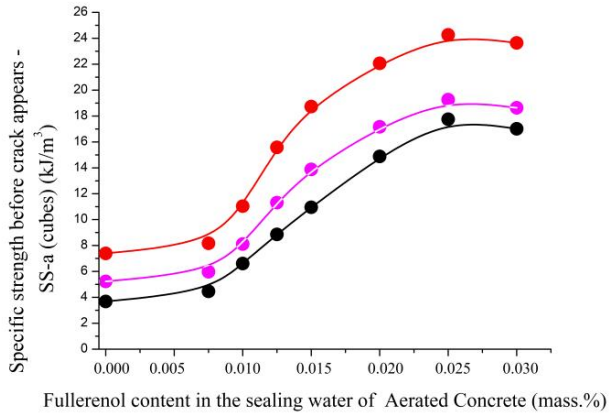

(**a**)

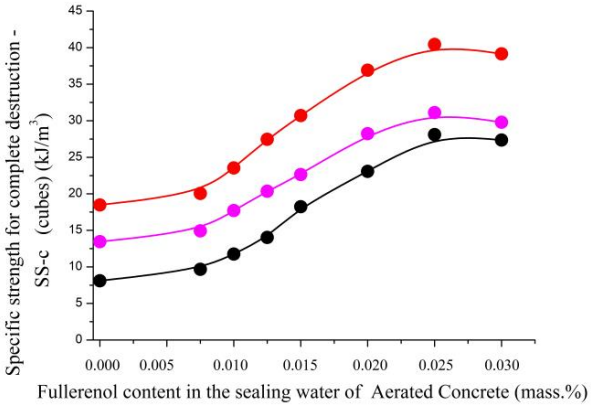

(**b**)

Figure 17. *Cont.*

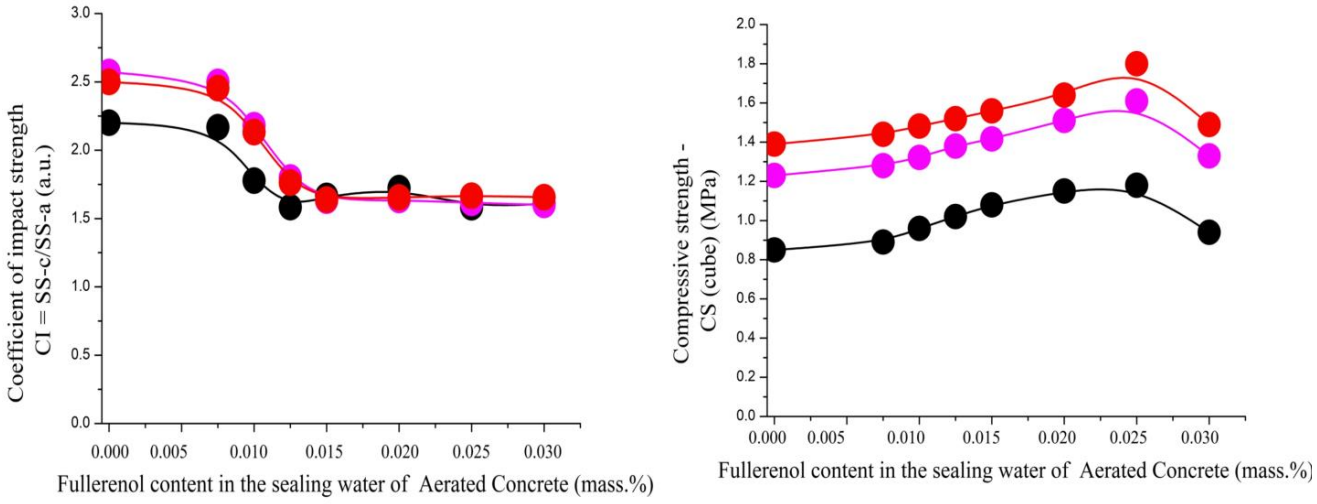

(**c**) (**d**)

Figure 17. The dependence of the strength characteristics of aerated concrete nanostructured with fullerenols: (**a**) specific strength before crack appears (top); (**b**) specific strength for complete destruction (middle); (**c**) coefficient of impact strength (bottom); (**d**) compressive strength of fullerenol content in sealing water at different mass ratios of cement ash/slag waste/lime: 1.0/1.0/0.0 (black); 1.0/0.9/0.1 (magenta); 1.0/0.8/0.2 (red).

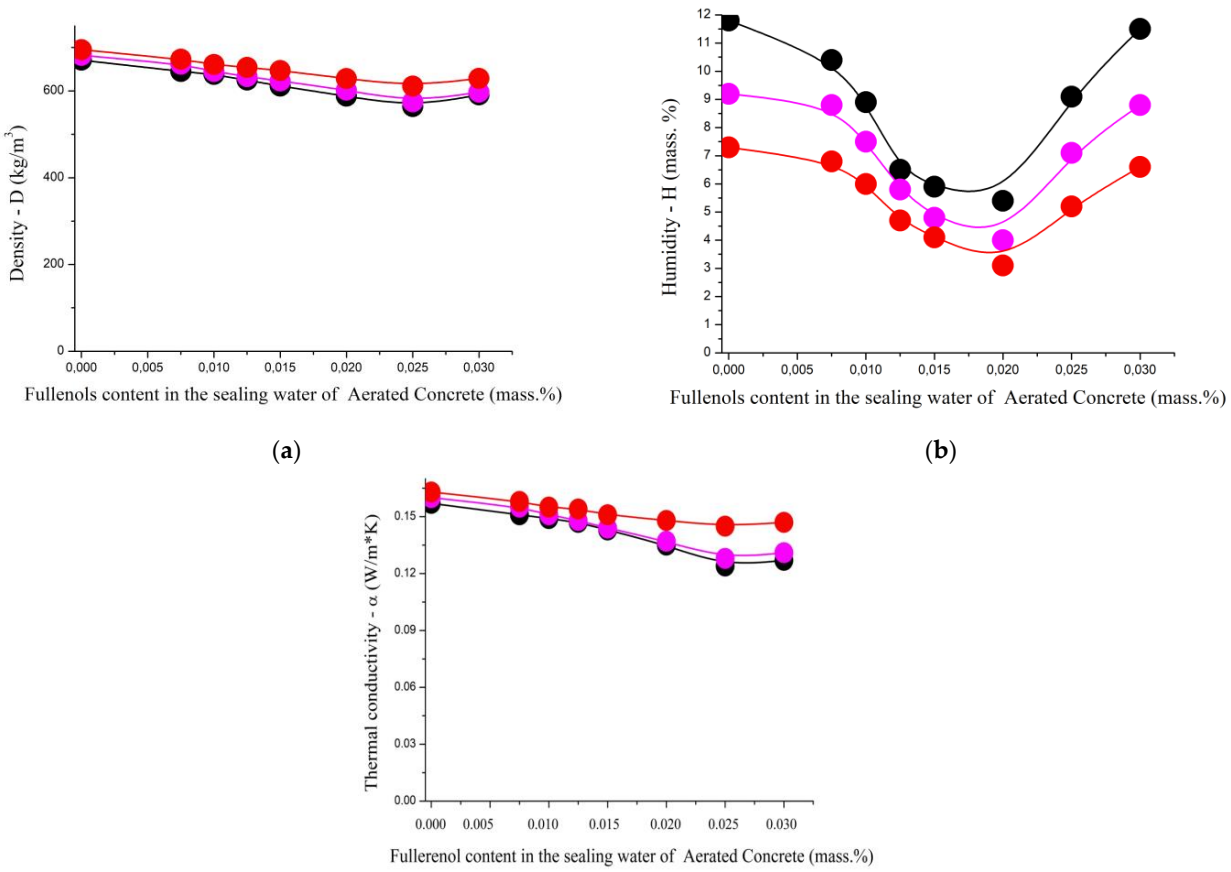

(**a**) (**b**)

(**c**)

Figure 18. The dependence of some properties of aerated concrete nanostructured with fullerenols, namely the (**a**) density (middle top), (**b**) humidity (middle bottom), and (**c**) thermal conductivity (bottom), on the fullerenol content in the sealing water at different mass ratios of cement ash/slag waste/lime: 1.0/1.0/0.0 (black); 1.0/0.9/0.1 (magenta); 1.0/0.8/0.2 (red).

4. Discussion

The increase in the influence of the nanopreparation added during the synthesis of the aerated concrete samples on their physical and mechanical characteristics is well demonstrated by Figures 17 and 18.

The dependencies presented in Figure 17a,b,d have the same configuration, showing an increase in the strength characteristics of the aerated concrete with the amount of the added nanopreparation. The maximum values are achieved at a *fullerenol-m* concentration of 0.022–0.028% based on the mass of the cement.

The dependencies of the density and thermal conductivity of the aerated concrete (Figure 18a,c) also have similar configurations. With an increase in the amount of the added nanopreparation, the strength and thermal conductivity of the aerated concrete decrease. The maximum decrease is achieved at a fullerenol concentration of 0.022–0.028% based on the mass of the cement.

In Figure 19, we present the most significant changes in the strength and some physical characteristics of the fullerenol-m-modified aerated concrete in comparison with unmodified samples against the fullereneol-m concentration in the sealing water.

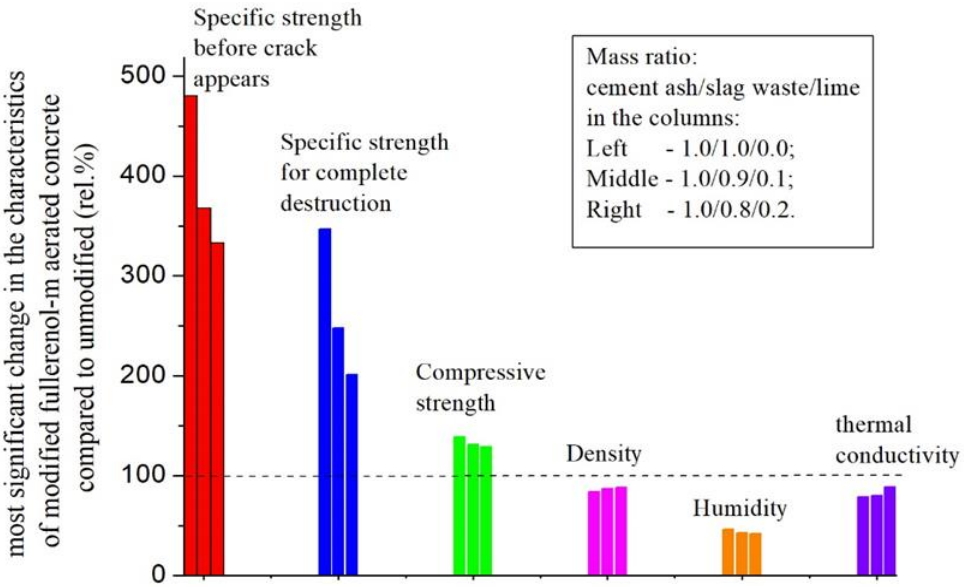

Figure 19. Most significant changes in the strength and some physical characteristics of *fullerenol-m*-modified aerated concrete in comparison with unmodified samples against *fullereneol-m* concentration in sealing water (mass ratio of cement ash/slag waste/lime in the column: 1.0/1.0/0.01—left, 1.0/0.9/0.1—middle, 1.0/0.8/0.2—right).

We can see that the introduction of water-soluble *fullerenol-m* into the composition of aerated concrete (in quantities of 0.0075–0.03 mass.%) has a significant effect on the strength and physicochemical properties of the concrete:

- The specific impact strength increases ≈3 ÷ 5 times (crack appears, maximum effect);
- The specific impact strength increases ≈2 ÷ 3 times (complete destruction);
- The compressive strength increases by ≈20 ÷ 30 rel.%;
- The density decreases by ≈12 ÷ 16 rel.%;
- The humidity decreases by ≈55 ÷ 60 rel.%;
- The thermal conductivity decreases by ≈10 ÷ 20 rel.%.

The maximum effect of the modification was observed with the minimal introduction of quicklime or in the absence thereof. All effects are positive regarding the exploitation characteristics of aerated concrete.

The conducted studies have shown the possibility of obtaining aerated concrete samples with improved characteristics, i.e., with increased strength and with a reduced density and thermal conductivity.

5. Conclusions

Thus, the introduction of water-soluble *fullerenol-m* into the composition of aerated concrete in micro-quantities has a significant positive effect on the specific impact strength (maximum increase is 3–5 times) and humidity (maximum decrease is 2–2.5 times) and has also a positive effect on the compressive strength, density and thermal conductivity (decrease is tens rel. %).

The effect of the additive's introduction is extreme. It is the maximum at a *fullerenol-m* concentration of 0.022–0.028 wt.% in relation to the mass of the cement, which corresponds to the minimum introduction of quicklime.

We believe that the unexpectedly strong effect of extremely low fullerenol-m concentrations on the strength and other physicochemical properties of aerated concrete is due to the strong structuring effect of even insignificant amounts of fullerenol-m on the sealing aqueous solution. Thus, it was previously experimentally shown (by densimetry) that, even in very dilute fullerenol solutions, the partial molar volumes of fullerenol have huge negative values, which are ten times higher in modulus than the average molar volume of fullerenol. This indirectly indicates the very strong ordering of aqueous solutions by fullerenols, partly due to the formation of a strong system of hydrogen bonds.

Author Contributions: Conceptualization, O.V.R., N.A.K. and M.A.S.; methodology, N.A.K., N.A.C. and D.K.A.; validation, O.V.R., N.A.K., N.A.C., M.A.S., D.K.A. and E.K.; formal analysis, O.V.R., M.A.S. and E.K.; investigation, O.V.R., N.A.K., M.A.S. and D.K.A.; resources, N.A.C. and N.A.K.; data curation, O.V.R.; writing—original draft preparation, O.V.R.; writing—review and editing, O.V.R., N.A.K., M.A.S. and N.A.C.; supervision, O.V.R. and D.K.A.; project administration, O.V.R., D.K.A. and E.K.; funding acquisition, O.V.R. and E.K. All authors have read and agreed to the published version of the manuscript.

Funding: The study was supported by the Science Committee of the Ministry of Science and Higher Education of the Republic of Kazakhstan and financed by grant No. BR21882292—"Integrated development of sustainable construction industries: innovative technologies, production optimization, efficient use of resources and creation of a technology park".

Data Availability Statement: The data presented in this study are available in this article (tables and figures).

Conflicts of Interest: The authors declare no conflicts of interest.

References

1. Sabitov, Y.Y.; Dyussembinov, D.S.; Zhumagulova, A.A.; Bazarbayev, D.O.; Lukpanov, R.E. Composite non-autoclaved aerated concrete based on an emulsion. *Mag. Civ. Eng.* **2021**, *106*, 10605. [CrossRef]
2. Li, H.; Zhang, M.; Ou, J. Abrasion resistance of concrete containing nano-particles for pavement. *Wear* **2006**, *260*, 1262–1266. [CrossRef]
3. Saleem, H.; Zaidi, S.J.; Alnuaimi, N.A. Recent Advancements in the Nanomaterial Application in Concrete and Its Ecological Impact. *Materials* **2021**, *14*, 6387. [CrossRef]
4. Yadav, S.; Saleem, H.; Ibrar, I.; Naji, O.; Hawari, A.A.; Alanezi, A.A.; Zaidi, S.J.; Altaee, A.; Zhou, J. Recent developments in forward osmosis membranes using carbon-based nanomaterials. *Desalination* **2020**, *482*, 114375. [CrossRef]
5. Huseien, G.F. A Review on Concrete Composites Modified with Nanoparticles. *J. Compos. Sci.* **2023**, *7*, 67. [CrossRef]
6. Alhassan, M.; Alkhawaldeh, A.; Betoush, N.; Alkhawaldeh, M.; Huseien, G.F.; Amaireh, L.; Elrefae, A. Life Cycle Assessment of the Sustainability of Alkali-Activated Binders. *Biomimetics* **2023**, *8*, 58. [CrossRef] [PubMed]
7. Hou, L.; Li, J.; Lu, Z.; Niu, Y. Influence of foaming agent on cement and foam concrete. *Constr. Build. Mater.* **2021**, *280*, 122399. [CrossRef]
8. Gołaszewski, J.; Klemczak, B.; Smolana, A.; Gołaszewska, M.; Cygan, G.; Mankel, C.; Peralta, I.; Röser, F.; Koenders, E.A.B. Effect of Foaming Agent, Binder and Density on the Compressive Strength and Thermal Conductivity of Ultra-Light Foam Concrete. *Buildings* **2022**, *12*, 1176. [CrossRef]

9. Al-Saffar, F.; Wong, L.; Paul, S. An Elucidative Review of the Nanomaterial Effect on the Durability and Calcium-Silicate-Hydrate (C-S-H) Gel Development of Concrete. *Gels* **2023**, *9*, 613. [CrossRef] [PubMed]
10. Yakovlev, G.; Kerien, J.; Plechanova, T.; Krutikov, V. Nanobewehrung von Schaumbeton. Beton- und Stahl. *Строительные Материалы* **2007**, *102*, 120–124.
11. Sanchez, F.; Sobolev, K. Nanotechnology in concrete—A review. *Constr. Build. Mater.* **2010**, *24*, 2060–2071. [CrossRef]
12. Urkhanova , L.A.; Rosina, V.E. High-Strength Concrete with the Use of Fly Ash and Microsilica. Proceedings of Irkutsk State Technical University. 2011. № 10. С. 97–100. Available online: https://journals.istu.edu/vestnik_irgtu/journals/2011/10 (accessed on 8 July 2024).
13. Fediuk, R.S.; Yushin, A.M. The use of fly ash the thermal power plants in the construction. *IOP Conf. Ser. Mater. Sci. Eng.* **2015**, *93*, 012070. [CrossRef]
14. Zolotarev, A.; Lushin, A.; Charykov, A.; Semenov, K.; Namazbaev, V.; Keskinov, V.; Kritchenkov, A. Impact Resistance of Cement and Gypsum Plaster Nanomodified by Water-Soluble Fullerenols. *Ind. Eng. Chem. Res.* **2013**, *52*, 14583–14591. [CrossRef]
15. Podolsky, N.E.; Lelet, M.I.; Ageev, S.V.; Petrov, A.V.; Mazur, A.S.; Iamalova, N.R.; Zakusilo, D.N.; Charykov, N.A.; Vasina, L.V.; Semenov, K.N.; et al. Thermodynamic properties of the C70(OH)12 fullerenol in the temperature range T = 9.2 K to 304.5 K. *J. Chem. Thermodyn.* **2020**, *144*, 106029. [CrossRef]
16. Sharoyko, V.V.; Ageev, S.V.; Meshcheriakov, A.A.; Akentiev, A.V.; Noskov, B.A.; Rakipov, I.T.; Charykov, N.A.; Kulenova, N.A.; Shaimardanova, B.K.; Podolsky, N.E.; et al. Physicochemical study of water-soluble C60(OH)24 fullerenol. *J. Mol. Liq.* **2020**, *311*, 113360–113411. [CrossRef]
17. Semenov, K.N.; Charykov, N.A.; Keskinov, V.A.; Letenko, D.G.; Nikitin, V.A.; Namazbaev, V.I. Synthesis and identification of mixed fullerenol, obtained by the method of the direct oxidation of fullerene soot. *Russ. J. Phys.Chem.* **2011**, *65*, 1108–1115.
18. Kratschmer, W.; Lamb, L.D.; Fostiropoulos, K.; Huffman, D.R. *Solid C60: A New Form of Carbon*; Nature: London, UK, 1990; Volume 347, pp. 354–358.
19. Smalley, R.E.; Haufler, R.E. Electric arc Process for Making Fullerenes. United. States Patent № 5227038, 13 July 1993.
20. Gruzinskaya, E.A.; Keskinov, V.A.; Keskinova, M.V.; Semenov, K.N.; Charykov, N.A. Fullerenovaya Sazha Elektrodugovogo Sinteza. *Nanosistemy Fiz. Khimiya Mat.* **2012**, *3*, 83–90. (In Russia)
21. Hasanshin, I.Y.; Popkova, O.S. Synthesis of fullerene soot by plasma enhanced chemical vapour deposition in impulsing discharge at atmospheric pressure from liquid hydrocarbon. *Sci. J. Kuban State Agrar. Univ.* **2012**, *80*, 1–13.
22. Abduguev, R.M.; Alekhin, O.S.; Gerasimov, V.I.; Losev, G.M.; Nekrasov, K.V.; Nikonov, Y.A.; Charykov, N.A. Device for Producing a Fullerene-Containing Black // WO2005087662 (A1), МПК C01B31/02, № PCT/RU2005/000119; published 22.09.2005.
23. Abduguevб, R.M.; Alekhin, O.S.; Gerasimov, V.I.; Losev, G.M.; Nekrasov, K.V.; Nikonov, Y.A.; Soroka, A.I.; Charykov, N.A. Method for Production a Fullerene-Containing Black // WO2005070826 (A1), МПК C01B31/02, C09C1/48, № PCT/RU2005/000025; published 04.08.2005.
24. Federal Agency for Technical Regulation and Metrology of the Russian Federation Certificate of Approval of the Type of Measuring Instruments. Federal Agency for Technical Regulation of Metrology. Russia. Chelyabinsk. 2017.RU.C.28.059.A. N 45609. 49 P.
25. *GOST 25485-89*; Cellular Concretes. Technical Conditions. State Construction Committee of the USSR: Moscow, Russia, 1990; 36p.
26. Limited Liability Company "Special Design Bureau Stroypribor". *Humidity Meter Electronic Moisture Meter-MG4-U*; Federal Agency for Metrology: Chelyabinsk, Russia, 2015; 36p. (In Russia)
27. *GOST 30515*; The Interstate Council for Standardization, Metrology and Certification. CEMENTS General Technical Conditions: Moscow, Russia, 2013; 37p. (In Russia)
28. Limited Liability Company "Special Design Bureau Stroypribor". *Thermal Conductivity Meter ITP-MG4*; Federal Agency for Metrology: Chelyabinsk, Russia, 2020; 39p. (In Russia)
29. Brooks, J. Elasticity, shrinkage, creep and thermal movement. In *Advanced Concrete Technology*; Elsevier: Amsterdam, The Netherlands, 2003.